J Shoulder Elbow Surg (2023) ■, 1–8

ELSEVIER

Journal of Shoulder and Elbow Surgery

www.elsevier.com/locate/ymse

Stemless reverse humeral component neck-shaft angle has an influence on initial fixation

David E. Cunningham, BEng[a,b,*], Gregory W. Spangenberg, BEng[a,b], G. Daniel G. Langohr, PhD[a,b], George S. Athwal, MD, FRCSC[b,c], James A. Johnson, PhD[a,b,c,d]

[a]*Department of Mechanical Engineering, The University of Western Ontario, London, ON, Canada*
[b]*The Roth|McFarlane Hand and Upper Limb Centre, St. Joseph's Hospital, London, ON, Canada*
[c]*Department of Surgery, The University of Western Ontario, London, ON, Canada*
[d]*Department of Biomedical Engineering, The University of Western Ontario, London, ON, Canada*

Background: Stemless anatomic humeral components are commonly used and are an accepted alternative to traditional stemmed implants in patients with good bone quality. Presently, little literature exists on the design and implantation parameters that influence primary time-zero fixation of stemless reverse humeral implants. Accordingly, this finite element analysis study assessed the surgical implantation variable of neck-shaft angle, and its effect on the primary time-zero fixation of reversed stemless humeral implants.
Methods: Eight computed tomography–derived humeral finite element models were used to examine a generic stemless humeral implant at varying neck-shaft angles of 130°, 135°, 140°, 145°, and 150°. Four loading scenarios (30° shoulder abduction with neutral forearm rotation, 30° shoulder abduction with forearm supination, a head-height lifting motion, and a single-handed steering motion) were employed. Implantation inclinations were compared based on the maximum bone-implant interface distraction detected after loading.
Results: The implant-bone distraction was greatest in the 130° neck-shaft angle implantation cases. All implant loading scenarios elicited significantly lower micromotion magnitudes when neck-shaft angle was increased ($P = .0001$). With every 5° increase in neck-shaft angle, there was an average 17% reduction in bone-implant distraction.
Conclusions: The neck-shaft angle of implantation for a stemless reverse humeral component is a modifiable parameter that appears to influence time-zero implant stability. Lower, more varus, neck-shaft angles increase bone-implant distractions with simulated activities of daily living. It is therefore suggested that humeral head osteotomies at a higher neck-shaft angle may be beneficial to maximize stemless humeral component stability.
Level of evidence: Basic Science Study; Computer Modeling

Keywords: Stemless; neck shaft angle; arthroplasty; implant design; finite element; reverse shoulder arthroplasty; cuff tear arthropathy

Institutional review board approval was not required for this basic science study.

*Reprint requests: David E. Cunningham, BEng, 1151 Richmond St., London, ON N6A 3K7, Canada.

E-mail address: dcunni9@uwo.ca (D.E. Cunningham).

Reverse shoulder arthroplasty (RSA) implants have undergone a variety of design modifications since first introduced. Some modifications include press-fit stems, modularity, adjustments in neck-shaft angle, and onlay/inlay design features. One design feature, focused on

1058-2746/$ - see front matter © 2023 Journal of Shoulder and Elbow Surgery Board of Trustees. All rights reserved.
https://doi.org/10.1016/j.jse.2023.06.035

decreasing stress shielding and simplifying future revisions, has been the gradual shortening of the humeral stem.[30]

Although anatomic stemless shoulder arthroplasty implants are steadily becoming more popular, the use of stemless RSA implants is still limited, with very few published works reporting on the clinical and biomechanical performance of these novel implants.[1] Shorter humeral stem lengths have been shown to decrease stress shielding in periprosthetic bone by better mimicking natural force-transmission properties.[27] Stemless designs also benefit from the preservation of humeral bone stock, reduction of risk of periprosthetic fractures, and simplification of surgical technique.[26] However, these designs of humeral implant also pose several risks that emphasize the importance of primary fixation. Ultrashort implants or stemless humeral implants are more vulnerable to poor initial fixation, instability, or loosening than their stemmed counterparts, because of the reduced bone-implant contact area and lack of cortical bone contact.[1,26]

The primary method of achieving fixation in existing stemless RSA implants is via osseointegration (viz. bony ingrowth). In order for this bone-implant bonding to occur, the two surfaces are required to maintain limited relative motion (termed "micromotion"[11,22]) during the healing phase following surgery.[8] The tolerable threshold of shear micromotion is often quoted as 150 μm.[3,6,10,20,26] However, the threshold of tolerable micromotion has also been reported as a range of between 30 μm[15,20] and 750 μm.[12,20] Additionally, it is rational to postulate that any lift-off or distraction micromotion may well impede bone contact and hence ingrowth.

One modifiable technical factor with stemless RSA humeral implants is the resection inclination angle (or neck-shaft angle) of the humeral head. RSA systems with varied neck-shaft angles of between 127.5° and 155° are currently used. It has been found that decreasing the neck-shaft angle reduces the risk of scapular notching,[14] and that modifying the neck-shaft angle results in no significant differences in scapular spine strain.[16] In addition, it has previously been found that decreasing the neck-shaft angle significantly increases impingement-free range of motion,[35] providing incentive to decreasing the neck-shaft angle. However, there remains a lack of knowledge regarding the effect of the neck-shaft angle on primary implant fixation.

Computational methods have gained popularity in orthopedics because of their ability to estimate postoperative physical phenomena that are difficult to measure in vivo.[4-6,9,13,28,30,31] Numerous computational studies evaluating implant designs are available[4,27,28,30,34]; however, little to no literature has evaluated the effect of neck-shaft angle on primary reverse humeral implant fixation in silico. The present investigation, therefore, determined the effect of stemless reverse humeral component insertion neck-shaft angles on the primary time-zero stability of the implants. We hypothesized that increasing the neck-shaft angle would result in better implant stability and decreased micromotion at the implant-bone interface.

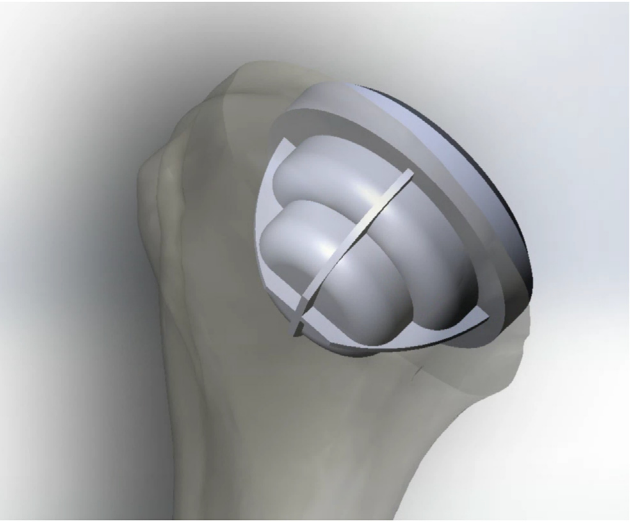

Figure 1 A posterior-lateral view of the left humerus implanted with a generic boundary-crossing implant, designed using variable-driven parametric design software. The implant was repetitively positioned into all 3D humeral models, developed from patient CT scans, at each neck-shaft angle.

Methods

Computed tomography (CT) scans of 8 shoulders from male cadaveric specimens (height: 177 ± 4 cm, weight: 69 ± 10 kg) aged 70 ± 21 years (mean ± standard deviation) were collected using a clinical CT scanner (slice thickness: 0.5 mm, pixel spacing: 0.961 × 0.961 mm, exposure time: 750 ms, kVp: 120) (GE 750HD Discovery Scanner; GE Healthcare, Chicago, IL, USA). A cortical bone surrogate (SB3 model 450; GAMMEX, Middleton, WI, USA) and distilled water were purposed as phantoms to calibrate the apparent density in grams per cubic centimeters from CT attenuation in Hounsfield units.[19] Three-dimensional models of the humerus (neck-shaft angle: 139° ± 6°, retroversion: 22° ± 13°) and cortical shell were created in Mimics (Materialise, Leuven, Belgium) and exported as nonuniform rational basis spline models instead of stereolithography models because they can model complex surfaces on the bony anatomy with greater accuracy. A Boolean subtraction was performed to isolate the trabecular bone model from the humeral model in a subsequent step.

A generic stemless reverse implant design was developed using CadQuery, a 3D parametric design Python library (Fig. 1).[25] This generic implant design was chosen as a general representation of a stemless boundary-crossing generic implant[4,30]; an amalgamation of the Reeves et al[30] Quad-Peg boundary crossing generic implant, as well as the Stryker Tornier, Zimmer Biomet, and Lima Corporate stemless designs currently available clinically. Anatomic generator implant examples were used because of the lack of stemless reversed implants available clinically. A single size of generic implant (glenosphere diameter: 40 mm, collar diameter: 36 mm, penetrating volume: 6.2 cm^3) was found to be an acceptable fit for all humeral models used.

The generic implant model was positioned by a board-certified surgeon (G.S.A.) in SolidWorks CAD software (Dassault Systèmes Corp., Waltham, MA, USA) at a 135° neck-shaft angle. In order to

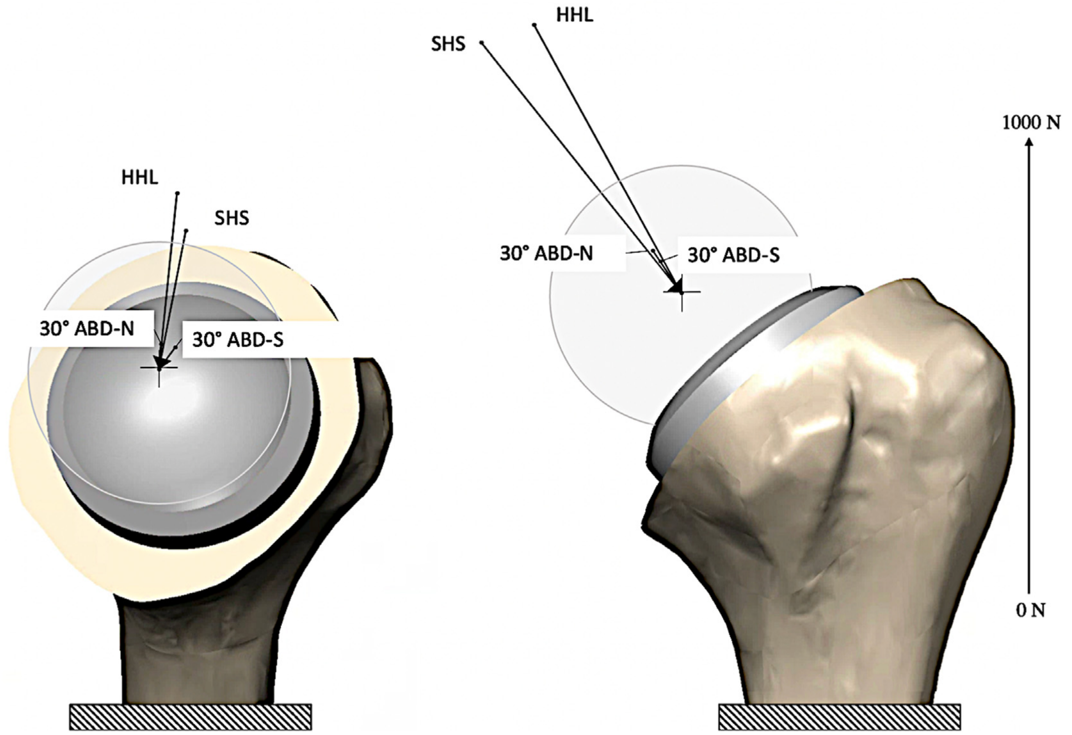

Figure 2 Four loading scenarios representing common activities of daily living that a patient might experience postoperatively (30° shoulder abduction with neutral forearm rotation [30° ABD-N], 30° shoulder abduction with forearm supination [30° ABD-S], a head-height lifting motion [HHL], and a single-handed steering motion [SHS]). Each load was applied to a point consistent with the center of the glenosphere in the reversed total shoulder arthroplasty reconstruction. Encastre boundary conditions are depicted at the distal humeral resection surface using striped boxes.

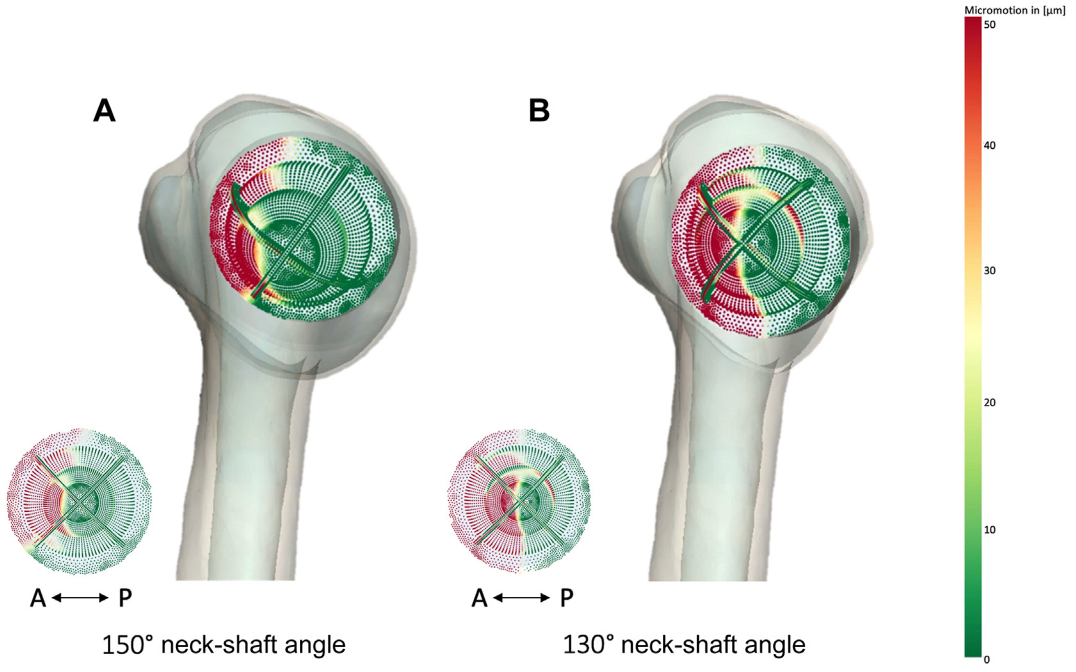

Figure 3 Posterior-lateral view of the left humerus, implanted with a generic stemless implant at 150° (**A**) and 130° (**B**), with a heatmap of bone-implant distraction magnitude overlayed. A lateral resection view is also displayed in the bottom left corner of each subplot. For illustration purposes, the micromotion heatmap resulting from a single-hand steering motion is shown.

ARTICLE IN PRESS

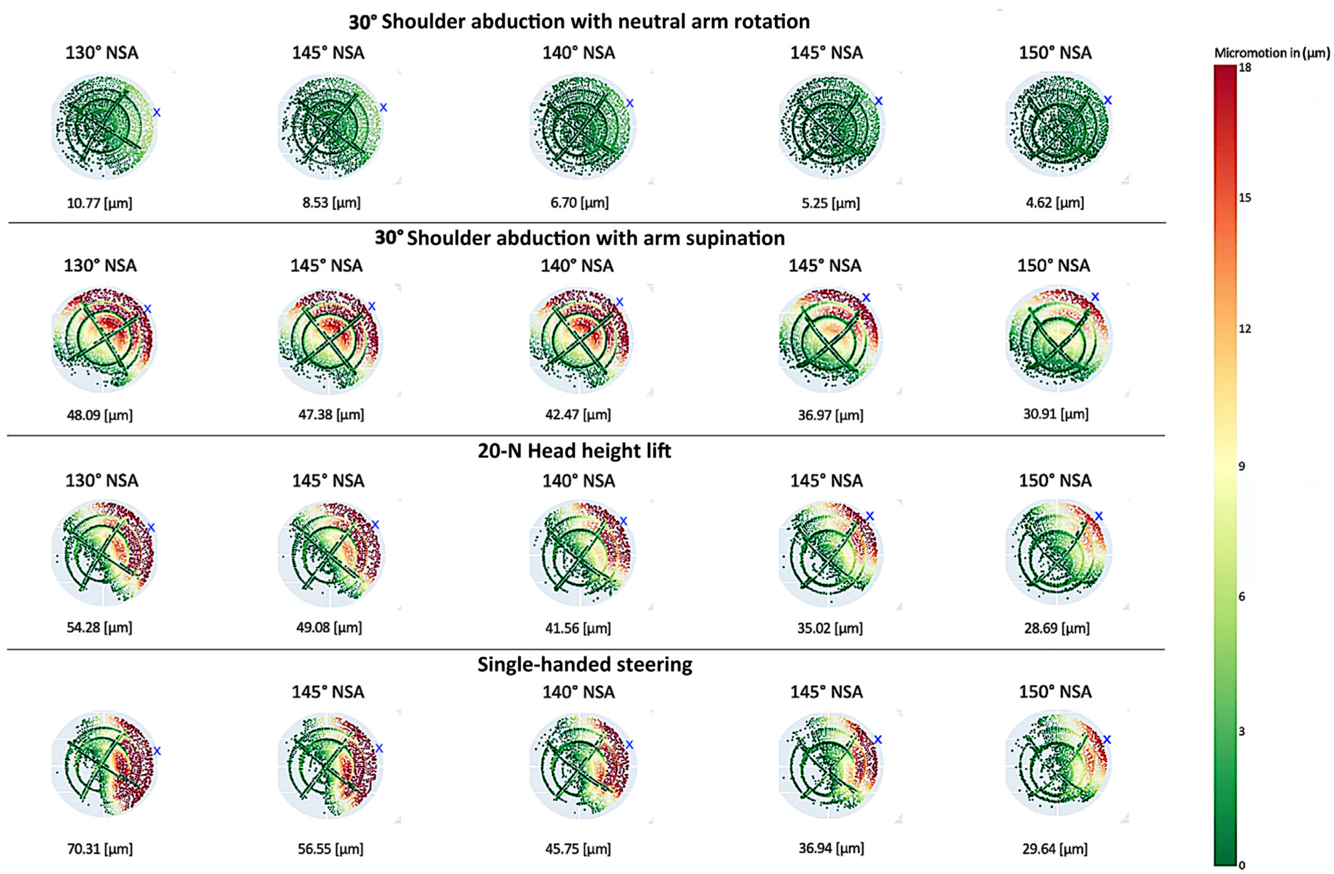

Figure 4 Heatmaps of the micromotions developed at the bone-implant interface (N = 1). All plots shown above are visualized medial-laterally at a view normal to the 135° neck-shaft angle (NSA) resection surface. Maximum micromotions were detected at the bone-implant interface at a position opposite to the direction of loading, indicated by the blue cross markings. Areas without colored nodes did not move relative to bone throughout the analysis.

maintain inclination consistency between specimens, the 135° implantation case was first positioned as a control, and a computational matrix transformation was used to vary the inclination angle (at 130°, 135°, 140°, 145°, and 150° neck-shaft angles). A constant center of rotation, positioned at the most superior-lateral apex of the anatomic humeral neck in each specimen, was identified in the 135° control resection and used for neck-shaft angle variation. Each humeral model was re-evaluated at every implantation condition. All implants were fully positioned in the humeral trabecular bone, and no cortical contact was detected.

Finite element models were developed in Abaqus CAE 2021 software (Dassault Systèmes Corp.) using a previously validated approach.[27-29] All components were meshed with 1.2-mm quadratic tetrahedral elements, according to mesh convergence. Cortical bone was assigned a constant Young modulus of 20 GPa,[18,23,28,30,32] and trabecular bone was assigned elastic moduli that varied in accordance to the Morgan et al[23] density-elasticity relationship.[19,21,28,30,32] Mimics CT software was utilized to apply all inhomogeneous material properties to trabecular bone models (0.11 ± 0.01 g/cm^3, Pearson skew: 1.87). The cortical and trabecular bone models were both assigned a Poisson ratio of 0.3.[6,28] The generic implant was assigned an elastic modulus of 110 GPa, representing titanium,[24,32] and a Poisson ratio of 0.3.[6,28,30] Implant-bone contact was assumed as frictional and modeled to represent the behavior of a titanium plasma-sprayed surface on bone ($\mu = 0.6$).[26]

We employed 4 different loading scenarios (30° shoulder abduction with neutral forearm rotation, 30° shoulder abduction with forearm supination, a head-height lifting motion, and a single-handed steering motion) built from Orthoload patient-based measurements[28] to encompass a range of activities, particularly those known to produce eccentric loading and, therefore, challenges to implant-bone fixation (Fig. 2). These aforementioned activities were chosen as they represent a diverse array of loading states that a patient may experience immediately postoperatively while adhering to standard postoperative instruction. Loading data were extracted and corrected for the individual body weight of each subject.[7,28,30] The joint force line of action was directed through the center of rotation of the simulated reverse arthroplasty joint, and the humeral models were assigned encastre boundary conditions on a plane 50 mm distal to the neck-shaft angle center of rotation (Fig. 2).

Analysis

In order to quantify the initial fixation of each implantation case, the maximum normal bone-implant distraction (micromotion) was assessed. A 1-way repeated measures analysis of variance (ANOVA) and a supplementary 2-way repeated measures ANOVA with Bonferroni correction were conducted for the dependent

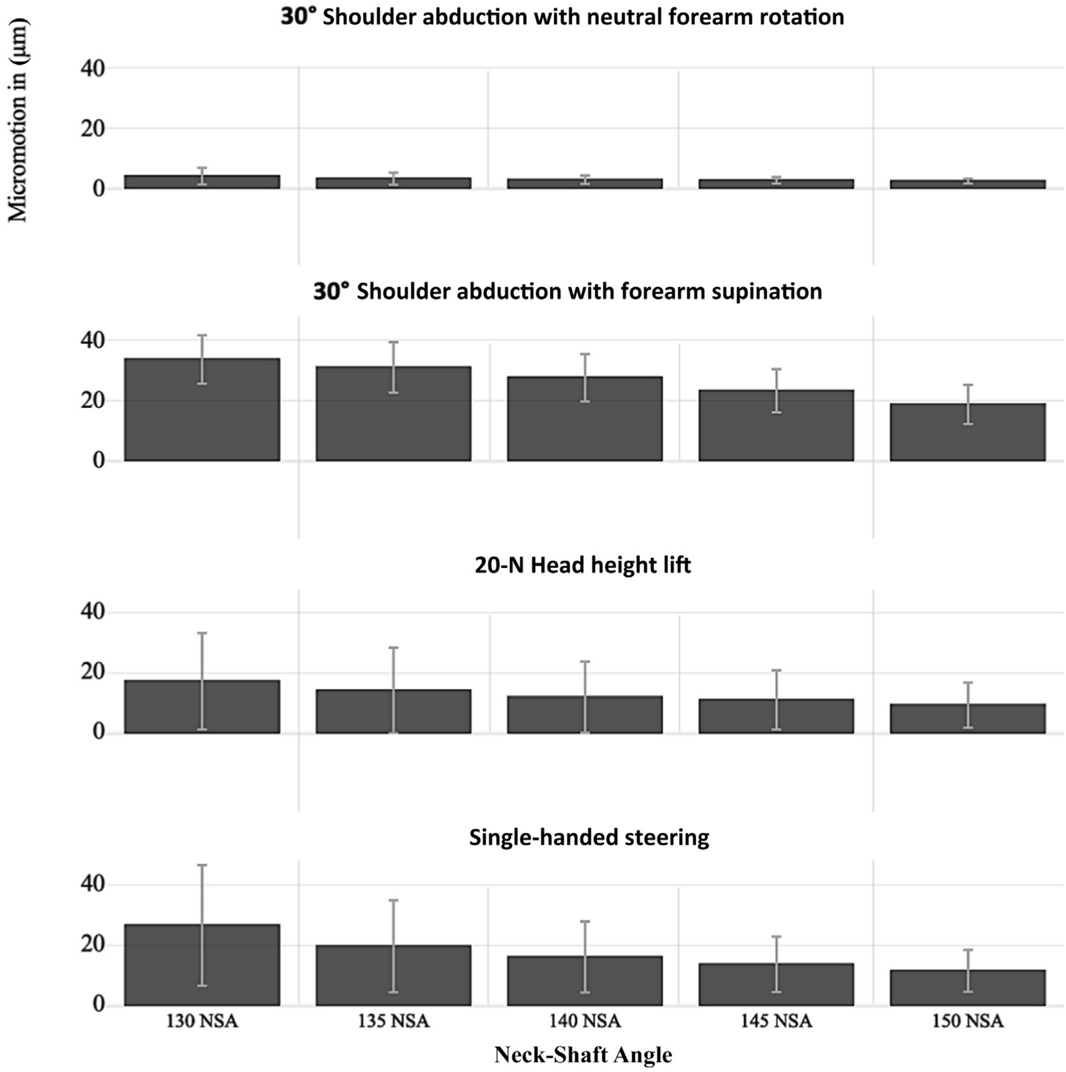

Figure 5 Maximum micromotion (mean ± 1 standard deviation) levels for the 4 simulated activities at 5 neck-shaft angles.

variable of neck-shaft angle for each loading scenario. All statistical analyses were computed using SciPy 1.9.1,[33] with the threshold of significance set as $P < .05$.

Results

Stemless humeral implants exhibit greater stability when implanted at higher neck-shaft angles. At higher neck-shaft angles, a larger portion of the implant maintained contact with the cancellous epiphyseal and metaphyseal bone (Fig. 3, *A*) when compared to lower, more vertical, neck-shaft angles (Fig. 3, *B*). For all loading cases, the maximum micromotion was detected on the periphery of the implant baseplate opposite to the direction of loading, whereas a greater portion of the implant maintained contact with bone at higher, more horizontal, neck-shaft angles (Fig. 4). The repeated measures ANOVA revealed that the maximum micromotion developed at the implant-bone interface was significantly higher for the 130° neck-shaft angle implantation conditions (30° shoulder abduction with neutral forearm rotation: $P = .0192$, 30° shoulder abduction with forearm supination: $P < .0001$, single-handed steering motion: $P = .0002$, head-height lifting motion: $P = .0038$) (Fig. 5, Table I). During a supplementary 2-way repeated measures ANOVA, Bonferroni correction with an adjusted alpha level of 0.025 (0.05/2) per test was used to further investigate the significance of neck-shaft angle. Results suggest that across all loading scenarios, the neck-shaft angle significantly affected initial implant stability ($P < .0001$).

With every 5° increase in neck-shaft angle, there was an average 14% decrease in the micromotion (30° shoulder abduction with neutral forearm rotation: 11.2%, 30° shoulder abduction with forearm supination: 13.5%,

Table I Interface micromotion parameters for varying implantation neck-shaft angles

	Micromotion (μm)									
	130°		135°		140°		145°		150°	
	Mean (SD)	Range	Mean (SD)	Range	Mean (SD)	Range	Mean (SD)	Range	Mean (SD)	Range
30° shoulder abduction with neutral forearm rotation	4.19 (2.77)	2.29-10.77	3.40 (1.99)	2.21-8.53	3.05 (1.43)	2.20-6.70	2.83 (1.07)	1.76-5.25	2.59 (0.80)	1.80-4.62
30° shoulder abduction with forearm supination	33.71 (8.01)	24.08-48.09	31.06 (8.36)	21.74-47.38	27.66 (7.86)	19.11-42.47	23.32 (7.15)	16.60-36.97	18.80 (6.50)	12.06-30.91
Single-handed steering motion	26.66 (19.94)	6.74-70.31	19.79 (15.16)	7.05-56.55	16.23 (11.70)	7.42-45.75	13.81 (9.12)	7.51-36.94	11.68 (6.92)	7.72-29.64
Head-height lifting motion	17.39 (15.96)	4.28-54.28	14.33 (14.12)	3.53-49.08	12.11 (11.71)	3.95-41.56	11.17 (9.79)	4.56-35.02	9.47 (7.45)	5.24-28.69

SD, standard deviation.
Each neck-shaft angle (130°-150°) was evaluated at loads representative of 4 activities of daily living.

single-handed steering motion: 18.5%, head-height lifting motion: 14.0%) developed during loading.

Discussion

The principal objective of this work was to assess how humeral resection inclination (or neck-shaft angle) may affect the primary stability of stemless reverse humeral implants. We specifically hypothesized that increasing neck-shaft angle, thereby decreasing implant inclination, would elicit a more favorable level of implant stability than is experienced at lower neck-shaft angles. Our results identified that variations in the neck-shaft angle substantially influence time-zero stemless implant fixation and stability.

From the results of this investigation, we postulate that increasing the neck-shaft angle and the potential improvement for stemless implant fixation may in part be attributed to the line of action of the joint loading vector relative to the implant-bone interface. With a more horizontal line of action (higher neck-shaft angle), the joint loading vector passes closer to the center of the interface, reducing eccentric loading. Hence, the implant experiences a greater amount of compression into the proximal humeral bone and less distraction or lift-off. With a more vertical neck-shaft angle, the implant does also experience compression; however, there is also a greater amount of eccentric loading. These eccentric loads, with a lower neck-shaft angle, result in substantially greater amount of distraction of the implant anteriorly. Distraction, as a mechanism of failure, would clinically present as lift-off of the implant anteriorly or flipping out of the implant.

We also postulate that bone quality may be influential, as altering the neck-shaft angle affects the native bone stock present at the bone-implant interface. Reeves et al[29] have shown that the best-quality bone in the proximal humerus is located peripherally in the metaphysis and in the humeral head. As such, we postulate that a higher neck-shaft angle resection preserves a wedge of higher-quality bone behind at the medial calcar region[29] (Fig. 6). Therefore, a stemless humeral implant placed at a higher neck-shaft angle is typically inset into better-quality bone in the medial calcar area than it would be at a lower neck-shaft angle.

Alterations in neck-shaft angle do have other important ramifications. Higher neck-shaft angles result in greater humeral distalization, adduction impingement, possible notching, reduced abduction impingement, and reduced internal/external rotation.[2,14] In contrast, lower neck-shaft angles result in greater humeral offset, improved adduction motion and rotation, and a higher potential for abduction impingement.[2,17] All of the above factors should be considered when selecting a particular neck-shaft angle.

There are limitations with the present work. A generic stemless implant design was assessed instead of implants currently available in the global market, which may lessen the clinical significance of these findings. The use of a

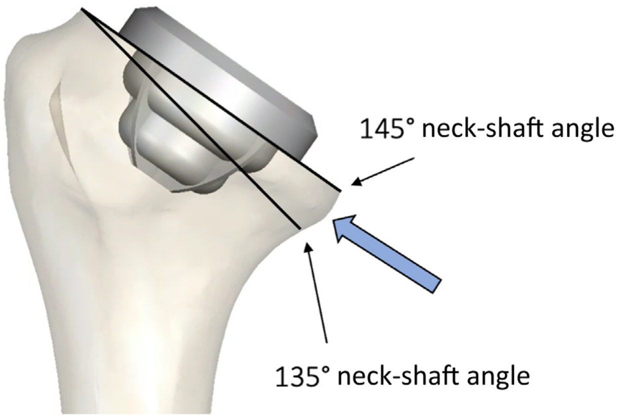

Figure 6 A stemless implant placed at a 145° neck-shaft angle. The resultant resection at 145° leaves a wedge of higher-quality medial calcar bone behind (*blue arrow*) for improved implant stability and fixation when compared with the 135° neck-shaft angle resection.

generic implant ensured that full control over implant variables could be maintained and could therefore align with the initial hypothesis. This provided unbiased insight into how neck-shaft angle may affect primary stability of stemless humeral implants. Future investigations should continue to assess additional implant designs in order to provide a more thorough evaluation on the load transfer effects of varying neck-shaft angles.

Another possible limitation of this work is the small sample size utilized. Future investigations should use a larger cohort of patient CTs in order to better represent the global population. However, the use of 8 specimens is higher than typically employed for computational studies of this nature on implant-bone stress analyses. Additionally, this evaluation was focused on time-zero (directly after implantation) implant behaviors. This is noteworthy, as trabecular bone is mechanoresponsive, and the differences in loading postoperatively may result in changes to the osseointegration responses in bone during the postoperative rehabilitation period. Specifically, in press-fit implants, experimental analyses focused on the effect of cyclical loading may provide valuable insight into the failure mechanisms of stemless humeral implants.

Strengths of this work include the repeated measures study design, with each specimen reconstructed repeatedly with varying neck-shaft angles. This produced a more robust statistical power. The loads applied were also based on in vivo telemetered data. Although these data were collected for an anatomic total shoulder arthroplasty implant, in vivo data for RSA do not yet exist. The same general loading scenarios adapted for RSA kinematics should not be markedly different.

Conclusion

The neck-shaft angle of implantation for a stemless reverse humeral component is a modifiable parameter that has a substantial effect on time-zero implant stability. Lower, more varus, neck-shaft angles increase bone-implant distractions with simulated activities of daily living. It is therefore suggested that in cases where primary reverse stemless implant stability is to be maximized for fixation, humeral head osteotomies at a higher neck-shaft angle may be beneficial.

Acknowledgments

The authors acknowledge support provided by Natural Sciences and Engineering Research Council of Canada, the St. Joseph's Healthcare Roth McFarlane Hand and Upper Limb Center, and the University of Western Ontario, London, ON, Canada.

Disclaimers:

Funding: No funding was disclosed by the authors.
Conflicts of interest: George S. Athwal is a consultant for DePuy-Synthes and Tornier (Wright Biomedical) and has received research support from Tornier (Wright Biomedical). The other authors, their immediate families, and any research foundations with which they are affiliated have not received any financial payments or other benefits from any commercial entity related to the subject of this article.

References

1. Ajibade DA, Yin CX, Hamid HS, Wiater BP, Martusiewicz A, Wiater JM. Stemless reverse total shoulder arthroplasty: a systematic review. J Shoulder Elbow Surg 2022;31:1083-95. https://doi.org/10.1016/j.jse.2021.12.017
2. Arenas-Miquelez A, Murphy RJ, Rosa A, Caironi D, Zumstein MA. Impact of humeral and glenoid component variations on range of motion in reverse geometry total shoulder arthroplasty: a standardized computer model study. J Shoulder Elbow Surg 2021;30:763-71. https://doi.org/10.1016/j.jse.2020.07.026
3. ASTM. ASTM F2028-17 standard test methods for dynamic evaluation of glenoid loosening or disassociation; 2018. p. 1-15. https://doi.org/10.1520/F2028-17
4. Bae TS, Ritzer EE, Cho W, Joo W. Effect of fin length and shape of stemless humeral components in a reverse shoulder implant system: a FEA study. J Mech Sci Technol 2021;35:417-22. https://doi.org/10.1007/s12206-020-1241-x
5. Bankoff ADP. Biomechanical characteristics of the bone in: human musculoskeletal biomechanics. 2012:. p. 61-85. Available at: https://www.intechopen.com/books/advanced-biometric-technologies/liveness-detection-in-biometrics. Accessed December 25, 2019.
6. Bonnevialle N, Geais L, Müller JH, Berhouet J. Effect of RSA glenoid baseplate central fixation on micromotion and bone stress. JSES Int 2020;4:979-86. https://doi.org/10.1016/j.jseint.2020.07.004

7. Damm P, Dymke J. Orthoload Database Jul. Wolff Inst. 2021 [cited 2021 Jul 26]. Available at: https://orthoload.com/database/. Accessed July 26, 2021.
8. Favre P, Henderson AD. Prediction of stemless humeral implant micromotion during upper limb activities. Clin Biomech 2016;36:46-51. https://doi.org/10.1016/j.clinbiomech.2016.05.003
9. Favre P, Perala S, Vogel P, Fucentese SF, Goff JR, Gerber C, et al. In vitro assessments of reverse glenoid stability using displacement gages are misleading – recommendations for accurate measurements of interface micromotion. Clin Biomech 2011;26:917-22. https://doi.org/10.1016/j.clinbiomech.2011.05.002
10. Favre P, Seebeck J, Thistlethwaite PAE, Obrist M, Steffens JG, Hopkins AR, et al. In vitro initial stability of a stemless humeral implant. Clin Biomech 2016;32:113-7. https://doi.org/10.1016/j.clinbiomech.2015.12.004
11. Formaini NT, Everding NG, Levy JC, Santoni BG, Nayak AN, Wilson C. Glenoid baseplate fixation using hybrid configurations of locked and unlocked peripheral screws. J Orthop Traumatol 2017;18:221-8. https://doi.org/10.1007/s10195-016-0438-3
12. Goodman S, Wang J-S, Doshi A, Aspenberg P. Difference in bone ingrowth after one versus two daily episodes of micromotion: experiments with titanium chambers in rabbits. J Biomed Mater Res 1993;27:1419-24.
13. Hopkins AR, Hansen UN, Bull AMJ, Emery R, Amis AA. Fixation of the reversed shoulder prosthesis. J Shoulder Elbow Surg 2008;17:974-80. https://doi.org/10.1016/j.jse.2008.04.012
14. Jeon BK, Panchal KA, Ji JH, Xin YZ, Park SR, Kim JH, et al. Combined effect of change in humeral neck-shaft angle and retroversion on shoulder range of motion in reverse total shoulder arthroplasty – a simulation study. Clin Biomech 2016;31:12-9. https://doi.org/10.1016/j.clinbiomech.2015.06.022
15. Kawahara H, Kawahara D, Hayakawa M, Tamai Y, Kuremoto T, Matsuda S. Osseointegration under immediate loading: biomechanical stress-strain and bone formation-resorption. Implant Dent 2003;12:61-8. https://doi.org/10.1097/01.ID.0000034394.75768.E3
16. Kerrigan AM, Reeves JM, Langohr GDG, Johnson JA, Athwal GS. The influence of reverse arthroplasty humeral component design features on scapular spine strain. J Shoulder Elbow Surg 2021;30:572-9. https://doi.org/10.1016/j.jse.2020.06.011
17. Kim DM, Aldeghaither M, Alabdullatif F, Shin MJ, Kholinne E, Kim H, et al. Loosening and revision rates after total shoulder arthroplasty: a systematic review of cemented all-polyethylene glenoid and three modern designs of metal-backed glenoid. BMC Musculoskelet Disord 2020;21:1-16. https://doi.org/10.1186/s12891-020-3135-6
18. Knowles N. Improving material Mapping in Glenohumeral finite element models: a Multi-level evaluation. Electronic Thesis and Dissertation Repository. 2019. Available at: https://ir.lib.uwo.ca/etd/6100. Accessed May 25, 2022.
19. Knowles NK, Reeves JM, Ferreira LM. Quantitative Computed Tomography (QCT) derived Bone Mineral Density (BMD) in finite element studies: a review of the literature. J Exp Orthop 2016;3:36. https://doi.org/10.1186/s40634-016-0072-2
20. Kohli N, Stoddart JC, van Arkel RJ. The limit of tolerable micromotion for implant osseointegration: a systematic review. Sci Rep 2021;11:1-11. https://doi.org/10.1038/s41598-021-90142-5
21. Mahaffy MD. Examining reverse total shoulder arthroplasty baseplate fixation in patients with E2-type glenoid erosion keywords; 2018. Accessed May 11, 2020.
22. Martin EJ, Duquin TR, Ehrensberger MT. Reverse total shoulder glenoid baseplate stability with superior glenoid bone loss. J Shoulder Elbow Surg 2017;26:1748-55. https://doi.org/10.1016/j.jse.2017.04.020
23. Morgan EF, Bayraktar HH, Keaveny TM. Trabecular bone modulus-density relationships depend on anatomic site. J Biomech 2003;36:897-904. https://doi.org/10.1016/S0021-9290(03)00071-X
24. Navarro M, Michiardi A, Castaño O, Planell JA, Interface JRS, Navarro M, et al. Biomaterials in orthopaedics Biomaterials in orthopaedics. J R Soc Interface 2008;5:1137-58. https://doi.org/10.1098/rsif.2008.0151
25. Parametric Products. CadQuery. Available at: https://github.com/CadQuery/cadquery. Accessed February 20, 2021.
26. Quental C, Folgado J, Comenda M, Monteiro J, Sarmento M. Primary stability analysis of stemless shoulder implants. Med Eng Phys 2020;81:22-9. https://doi.org/10.1016/j.medengphy.2020.04.009
27. Razfar N. Finite Element Modeling of the Proximal Humerus to Compare Stemless, Short, and Standard Stem Humeral Components of Varying Material Stiffness for Shoulder Arthroplasty. London: Ontario: University of Western Ontario - Electronic Thesis and Dissertation Repository; 2014. Available at: https://ir.lib.uwo.ca/etd/2431
28. Razfar N, Reeves JM, Langohr DG, Willing R, Athwal GS, Johnson JA. Comparison of proximal humeral bone stresses between stemless, short stem, and standard stem length: a finite element analysis. J Shoulder Elbow Surg 2016;25:1076-83. https://doi.org/10.1016/j.jse.2015.11.011
29. Reeves JM. An in-silico assessment of stemless shoulder arthroplasty: from an in-silico assessment of stemless shoulder arthroplasty: from CT to predicted bone response CT to predicted bone response. 2018. Available at: https://ir.lib.uwo.ca/etdhttps://ir.lib.uwo.ca/etd/5398. Accessed April 9, 2021.
30. Reeves JM, Langohr GDG, Athwal GS, Johnson JA. The effect of stemless humeral component fixation feature design on bone stress and strain response: a finite element analysis. J Shoulder Elbow Surg 2018;27:2232-41. https://doi.org/10.1016/j.jse.2018.06.002
31. Suárez DR, Nerkens W, Valstar ER, Rozing PM, van Keulen F. Interface micromotions increase with less-conforming cementless glenoid components. J Shoulder Elbow Surg 2012;21:474-82. https://doi.org/10.1016/j.jse.2011.03.008
32. Synnott S. The effect of implant girth and implant collar on the degree of bone to implant contact and bone stresses in the proximal humerus; 2018. Accessed May 25, 2022.
33. Virtanen P, Gommers R, Oliphant TE, Haberland M, Reddy T, Cournapeau D, et al. SciPy 1.0: fundamental algorithms for scientific computing in Python. Nat Methods 2020;17:261-72. https://doi.org/10.1038/s41592-019-0686-2
34. Wahab AHA, Saad APM, Syahrom A, Kadir MRA. In silico study of glenoid perforation during total shoulder arthroplasty: the effects on stress & micromotion. Comput Methods Biomech Biomed Engin 2020;23:182-90. https://doi.org/10.1080/10255842.2019.1709828
35. Werner BS, Chaoui J, Walch G. The influence of humeral neck shaft angle and glenoid lateralization on range of motion in reverse shoulder arthroplasty. J Shoulder Elbow Surg 2017;26:1726-31. https://doi.org/10.1016/j.jse.2017.03.032